CHEMNANOMAT

CHEMISTRY OF NANOMATERIALS FOR ENERGY, BIOLOGY AND MORE

www.chemnanomat.org

Accepted Article

Title: Enhancing Epoxy Composites with Graphene and Graphene Oxide: Thermal and Mechanical Insights

Authors: Sławomir Wilczewski, Zdzislaw Nowak, Michał Maj, Magdalena Osial, Roman Minikayev, and Michael Giersig

To be cited as: *ChemNanoMat* **2024**, e202400488

Link to VoR: https://doi.org/10.1002/cnma.202400488

A Journal of

ACES Asian Chemical Editorial Society

WILEY VCH

10.1002/cnma.202400488

WILEY VCH

RESEARCH ARTICLE

Enhancing Epoxy Composites with Graphene and Graphene Oxide: Thermal and Mechanical Insights

Sławomir Wilczewski,[a] Zdzisław Nowak,*[b] Michał Maj,[c] Magdalena Osial,[b] Roman Minikayev,[d] and Michael Giersig*[b]

[a] S. Wilczewski
Faculty of Chemical Technology and Engineering,
Bydgoszcz University of Science and Technology
Seminaryjna 3, Bydgoszcz, Poland

[b] Z. Nowak, M. Osial, M. Giersig
Department of Theory of Continuous Media and Nanostructures
Institute of Fundamental Technological Research, Polish Academy of Sciences
A. Pawińskiego 5B, Warsaw, Poland
E-mail: znowak@ippt.pan.pl, mgiersig@ippt.pan.pl

[c] M. Maj
Department of Mechanics of Materials
Institute of Fundamental Technological Research, Polish Academy of Sciences
A. Pawińskiego 5B, Warsaw, Poland

[d] PhD R. Minikayev
Institute of Physics, Polish Academy of Sciences
Al. Lotników 32/46, Warsaw, Poland

Abstract: This paper shows the graphene and graphene oxide nanoflakes as the 0.1, 0.5, 1, 2, and 4 wt.% reinforcement of epoxy-resin matrix to enhance the thermal and mechanical characteristics of the composite. Experimental measurement of the glass transition temperature and thermal expansion coefficient indicated that the addition of nanostructural filler improving the glass transition temperature about ~12 ºC for nanocomposite filled carbon-based nanoparticles for both heating and cooling cycles compared to the bare epoxy resin. Young's elastic modulus measured by nanoindentation and the stress versus strain curves for different weight fractions of graphene nanoflakes additives during uniaxial compression and tension considered were obtained from the experiments. The distributions of logarithmic strain field for the transverse, axial and shear components on the nanocomposites sample surfaces, during the uniaxial tension process for quasi-static strain rates, were analyzed. The tensile strengths show improvement for nanocomposites with less than 1 % weight fraction of carbon-based nanoparticles. The compressive yield stress increased to a maximal value (at the recorded peak on the curve) for an epoxy nanocomposite having 2 wt.% oxidized graphene flakes, where both parameters were enhanced with the oxidized form of graphene for the more effective dispersion in the epoxy resin matrix over the bare graphene filler.

Introduction

Nano-reinforced polymers, particularly nanoparticles filled epoxy resin (EP), have received significant attention in recent decades. Epoxy resins as a matrix belong to a thermosetting polymers used extensively in bonded joints, protective corrosion coatings, structural and electronic components [1, 2]. These materials, due to their highly cross-linked structure, are characterized by good mechanical properties, dimensional stability, heat and chemical resistance [3, 4]. However, they are brittle due to their high internal cross-linking, which significantly limits their further application development. Therefore, reinforcing materials used in EP are extremely important and have been extensively researched. Nanostructural fillers can offer a range of features (shape, and concentration) to modify/enhance the thermal and mechanical properties of epoxy matrices. By choosing an appropriate combination of epoxy matrix and reinforcement dopant, a new material can be made that exactly meets the requirements of a certain application. Over the past few decades, various modifiers have been developed to improve the properties of epoxy resins include; rubber particles, thermoplastic polymers, core-shell particles, hyper branched polymers and various types of reinforcing fibers. Recently, several works have demonstrated the incorporation of the graphene fillers into epoxy resin to form the nanocomposites, indicating that the modulus and glass transition temperature (T_g) of the nanocomposites can be effectively increased [5, 6]. Wang et al. [5] investigated the thermal properties of graphene nanocomposites, revealing that graphene can effectively improve the thermal stability of epoxy polymer. Where

the addition of 5% filler reduced the coefficient of thermal expansion below the glass transition temperature, relative to the matrix material by 31.7%. Tang et al. [6] investigated the effect of graphene dispersion on the mechanical properties of nanocomposites. It was shown in [6] that nanocomposites with high homogeneity show higher strength and fracture toughness than those in which filler agglomerations were observed. However, achieving satisfactory property improvements, e.g. for the glass transition temperature, thermal exponent coefficient and thermal conductivity, usually involves the use of high filler percentages of up to 60 % of the nanocomposite volume [1, 7, 8]. Polymer-based nanocomposites with carbon nanostructures as fillers, offer great prospects in constructional applications thanks to their relatively high mechanical properties (per unit mass) [9, 10, 11] and [12]. Graphene (GN) and graphene oxide (GO) are carbon materials that have been developed relatively in recent studies. Graphene an allotropic form of carbon, has many unique properties that include a Young's modulus of approximately 1 TPa, a tensile strength of 130 GPa, exceptional optical properties (graphene can absorb 2.3 % white light), excellent thermal conductivity of 4840 to 5300 $Wm^{-1}K^{-1}$ and an electrical resistivity of 10^{-3} Ωcm^{-1} [13-15]. The effectiveness of graphene as a nanofiller in resin or metal matrix nanocomposites systems has been reported in [8,16-19]. Graphene oxide, an oxidized form of GN as a potential filler for polymer-based nanocomposites, has many advantages over graphene due to the presence of oxygen functional groups on its surface [2, 20-23].

The methods presented in the literature for obtaining graphene or oxide graphene reinforced EP nanocomposites are based on different ways of introducing graphene into the polymer matrix like the simplest methods involving mixing of the resin, hardener and filler as well as the dispersion of the nanoparticles in the organic or inorganic solvents containing resin without hardener with subsequent evaporation of the solvent and the addition of the hardener; or the heating of the solution prior to the crosslinking [24-29]. In many studies, modifications of the basic preparation method have been used to improve the dispersion of GN or GO in the nanocomposites. These modifications consisted in heating the polymer during mixing [30] or on pre-dispersion of the filler in a solvent [1, 3, 31-32]. In addition to methods for obtaining nanocomposites with a disordered dispersion of GO and GN throughout the nanocomposite, studies are also known in which layered materials or nanocomposites with a graphene scaffold were obtained [7, 24, 29, 35-36]. In the first method, a layer of graphene was flooded with resin and, after curing, another layer prepared in the same way was added. In the second, a graphene scaffold was prepared using a freeze-drying process, which was then embedded in EP.

Epoxy resin-based nanocomposites with graphene and graphene oxide have a number of interesting effects in terms of improved properties. These include higher tensile strength and Young's modulus, higher thermal and electrical conductivity, better tribological properties, lower flammability and better corrosion properties of resin protective coatings [28, 29, 37]. Therefore, the studies intensified on the exploration of particle-matrix interactions, highlighting the need to understand these interactions at the molecular level and their impact on the physicochemical properties of the resulting nanocomposite. In this study, the presence of oxygen atoms on graphene flakes facilitated favorable conditions for hydrogen bonding interactions, contributing to improved locally ordered structure and π-π interactions with the polymer matrix. The identified mechanical response features provide the basis for the development of constitutive models tailored for graphene-enriched composite nanocomposites. Based on the results presented here, it is possible to propose numerical models using deterministic or stochastic modeling methods to study the internal progressive softening and curing of epoxy resin-based nanocomposites and carbon nanostructures. Therefore, the works devoted to this issue are part of the latest trends in the study of these materials [38-45].

In this work, we presented the effect of mechanical and thermal properties of the nanocomposite based on the epoxy resin matrix filled with the GN and GO fillers on the tensile and compression performance with pointing out the contribution of factors such as reinforcement of nanoparticles into the resin matrix as the step forward the reduction of the composite mass with the addition of the nanoparticles instead of the larger reinforcements that are proposed in the literature, improving the thermal stability, and the increase of the loading of the composites with maintaining the green approach in the composites production.

Experimental

Materials

The graphene-epoxy nanocomposites used in this study were obtained using resin Epoxidharz L20 and hardener EPH 161 (R\&G Faserverbundwerkstaffe GmbH) (EP L20 Waldenbuch, Germany). Graphene nanoflakes xGNP-M-5 (XG Science) (CAS: 7782-42-5), Lansing (Michigan), USA was used as a filler. Sulfuric acid (H_2SO_4) (95%) (CAS: 7664-93-9) and nitric acid (HNO_3) (65%) (CAS: 7697-37-2) (Avantor Performance Materials Poland S.A., Gliwice, Poland) were used for oxidation of graphene.

Preparation of EP L20/graphene nanocomposites

In the first stage, of preparation of the nanocomposites certain amounts of resin and hardener as well as graphene were weighed in the amount of 0.1, 0.5, 1, 2, 4 wt.%. In the second stage, the filler was mixed magnetically with the resin for 10 min with an average speed of 900 rpm. Then, the hardener was added and mixed at the same rate for another 2 min. The resulting mixtures were degassed under vacuum (-1 bar) and poured into silicone molds. Composites, as recommended by the manufacturer were left under the room temperature for 24 h for cross-linking, then the materials were heated at 100 °C for 24 h to finish cross-linking process. The resin without graphene was obtained under the same conditions as the reference test. Scheme of nanocomposites manufacturing was shown on Figure 1.

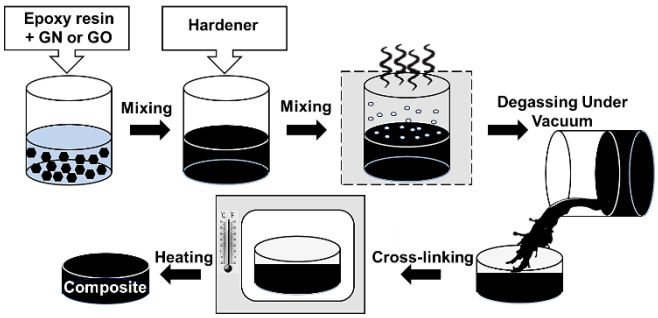

Figure 1. Scheme of nanocomposites manufacturing.

Preparation of EP L20/oxidized graphene nanocomposites

In the first stage of preparation of the nanocomposites, graphene was oxidized to avoid any erroneous coordination of the surface oxygen atoms with a mixture of H_2SO_4 and HNO_3 in a volume ratio (3:1). GN (1.5 g) was added to 600 cm^3 of the acid mixture, then the solution was stirred for 30 min at 500 rpm and sonicated for 30 min in an ultrasonic bath at 60 °C (the mixing and sonication cycle was repeated three times). In the next stage, the dispersion of filler in the mixture of acids was left for 14 h. After the mixture was diluted 4 times with distilled water and filtered under reduced pressure on a filter with 0.45 μm pores. The obtained filler was centrifuged 5 times in distilled water at 9000 rpm for 3 min and dried at 50 °C for 96 h. As an effect, the oxidized graphene (GO) flakes were obtained. The GO-based nanocomposites were achieved within the procedure described in previous Section. In following Sections labels of EP L20 neat, EP L20+0.1 wt.% GN, EP L20+0.5 wt.% GN, EP L20+1 wt.% GN, EP L20+2 wt.% GN and EP L20+4 wt.% GN signifies epoxy nanocomposites reinforced with 0, 0.1, 0.5, 1, 2, and 4 wt.% of GN. However, the labels EP L20+0.1 wt.% GO, EP L20+0.5 wt.% GO, EP L20+1 wt.% GO, EP L20+2 wt.% GO and EP L20+4 wt.% GO indicates epoxy nanocomposites reinforced with 0, 0.1, 0.5, 1, 2, and 4 wt.% of GO, respectively.

Methods

Prior to the nanocomposites fabrication, the morphology of carbon-based nanoflakes was investigated using scanning electron microscopy (SEM) (Zeiss Crossbeam 350 microscope, Stuttgart, Germany). Complementary, the High Resolution Transmission Electron Microscopy (HRTEM) (Philips CM 12, Eidenhoven, the Netherlands) was used to check the crystallinity of the graphene filler. The incorporation of the of GN and GO fillers into the epoxy-resin was investigated by Fourier transform infrared spectroscopy (FT-IR) using ATR technique. The study was carried out with a Bruker Alpha instrument in the range of 4000-400 cm^{-1}. A total of 32 scans were performed at a resolution of 4 cm^{-1}. Complementary to the FT-IR analysis, the nanocomposite was also investigated using Raman DXR microscope (Thermo Fisher Scientific, Waltham, MA, USA) using laser line 532 nm, where the samples were measured with 50 repetitions of 50 s each (20 in successive control measurements). The aperture was 50 μm, the lenses were 10 and 50 mm, and the laser beam power was 1 mW.

The XRD measurements were performed on a laboratory diffractometer (X'Pert MPD, Panalytical) equipped with Cu x-ray tube and primary Johansson type (Ge) monochromator in the Bragg-Brentano geometry.

The stability of GN and GO dispersions in epoxy resin (0.1 wt.%) was measured by multiple light scattering using a Turbiscan Lab instrument (Formulaction SA, Toulouse, France), in which GN and GO suspensions in epoxy resin were placed in glass cylindrical measuring tubes with a working height of 54 mm and scanned at 880 nm. Scanning was carried out for 24 hours (once per hour) at room temperature, corresponding to crosslinking conditions. The Turbiscan Stability Index (TSI) was determined from the results through TurbiSoft-Lab-2.3.1.125 software. After 24 hours of scanning, digital images of the prepared dispersions were also taken.

Next, the thermal expansion of prepared nanocomposites was measured performed using a TMA 450 apparatus from TA Instruments in the temperature range of 25-200 °C in a heating and cooling cycle in a nitrogen atmosphere, and the temperature change rate of 2 °C min^{-1}. Based on the results obtained, the coefficients of thermal expansion (CTE) were determined (using

software provided by the manufacturer) in the temperature range below the glass transition temperature (25-80 °C) and above the glass transition temperature (125-180 °C) in both heating and cooling cycles. The glass transition temperature (T_g) was also determined as T_{onset} (heating cycle) and T_{endset} (cooling cycle) for the materials obtained. The curve presenting technique that was used is presented in Figure 2.

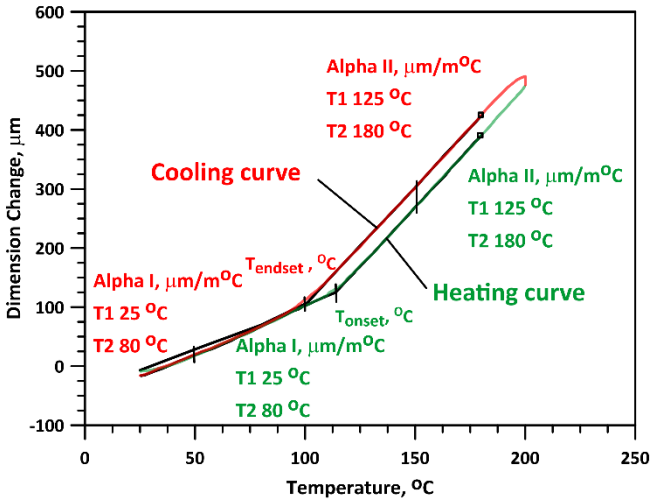

Figure 2. The method to determine Alpha I, Alpha II and glass transition temperature based on thermal expansion test.

The mechanical response of epoxy resin L20 GN and L20 GN GO doped graphene flakes have been studied in room temperature in quasi-static strain rate tension and compression. The samples used for tension tests were a dog-bone shape type and for compression tests were a cylindrical shape type, see Figure 3 (a, b). The cylindrical samples were with 9 mm diameter and machined to 14 mm in length to provide a diameter to length ratio of 0.64.

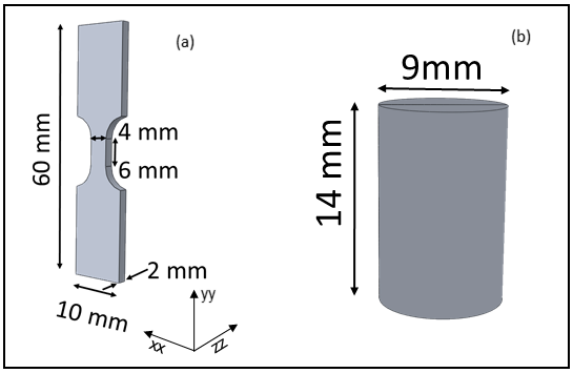

Figure 3. The uniaxial tension tests (a) and compression tests (b) sample shape and dimensions in mm.

Strains were measured by using a digital image correlation technique, and strain gages. Characteristic points of tensile and compressive stress strain relation such as proportional elastic limit stress (PEL), tensile strength and compressive yield strength (CYS) were discussed in Section: Mechanical properties studies. The bonding between the epoxy matrix and graphene flakes phases is considered to be perfect. The prepared samples were deformed using MTS 858 Mini Bionix II testing machine (MTS Systems Corporation, 14000 Technology Drive, Eden Praire, MN USA) under displacement controlled uniaxial deformation and taking into account the sample's geometry, they corresponded to the mean values of strain rate $\dot{\varepsilon}$ equal to 0.001 s^{-1}.

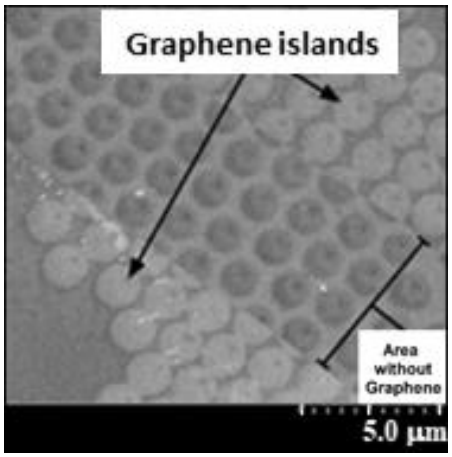

(a)

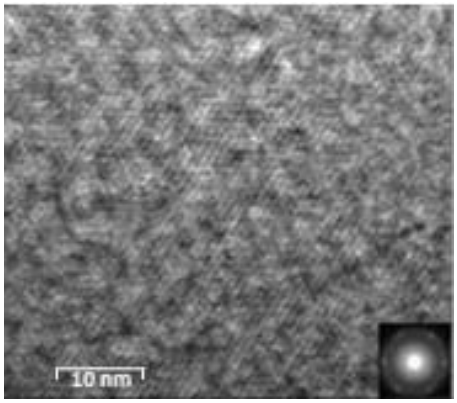

(b)

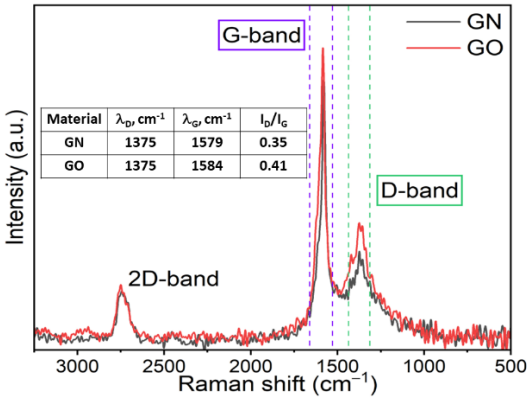

Material	λ_D, cm^{-1}	λ_G, cm^{-1}	I_D/I_G
GN	1375	1579	0.35
GO	1375	1584	0.41

(c)

Figure 4. Images on graphene flakes with a diameter of about 1.5 micron (a) the high crystallinity of the structure is shown in the HRTEM image (b), the quality of the crystal is also confirmed with Raman characterization (c) where the average 2D/G height ratio of 4.3 is presented.

Results

Morphology, composition, and stability studies

The morphology studies using HRTEM confirmed the uniform distribution of the graphene in the epoxy resin. As can be seen in the Figure 4 (a) the graphene islands can be distinguished in the polymer matrix, where the diameter of each island is about 1.5 μm. The samples were observed in high-resolution transmission electron microscopes, Phillips 12 and JEOL 4000, operating at 120 respectively 200 kV. The quality of the lattice images was improved using the conditions of minimum phase contrast according to Kunath [70].

In Figure 4b, the ultrastructure of the graphene plate is clearly resolved by HRTEM. The typical lattice plane is obvious, and the inserted FFT analysis further validates these structural features. In particular, the FFT spots provide clear insights into the phase and amplitude information, highlighting the crystallographic orientation and periodicity of the graphene lattice of the graphene filler.

As the Raman spectroscopy is a useful technique for studying graphene material composition, it was used to provide information on the structure, number of layers and exfoliation of the material [46]. Figure 4 (c) shows the presence of the peaks at about 1375 cm^{-1} that can be assigned to the D bands, while the peaks at 1579 cm^{-1} in GN and 1584 cm^{-1} in GO can be ascribed to the G bands. The G peak is related to the crystal structure of sp^2 carbon, while the D band provides information about defects and impurities in the graphene structure [46-47]. The band intensity ratio, I_D/I_G, is commonly used to estimate the size of the graphene domain and the relative degree of graphitization of the material. This value is inversely proportional to the size of the crystallites [48-49]. The results shown in Figure 4 (b) showed an increase in the intensity of the D band and the I_D/I_G intensity ratio, indicating the effective oxidation of graphene surface and an increase in the exfoliation of the GO structure relative to GN due to the chemical processes carried out. The stacking of layers in GN can be related to the position of the G-band peak shifts towards a lower Raman shift value [46]. In the GO spectrum shown in Figure 4 (b) the opposite situation was observed. The location of the G band of this material is shifted by 5 cm^{-1} in the direction of higher values compared to GN. The greater dispersion of GO was further confirmed by this fact. The obtained results of Raman spectroscopy analysis confirm the SEM observations which indicated an increase in GO exfoliation relative to GN. Figure 4 (c) reveals the image with atomic resolution of the particular graphene island. It is clearly seen that the material is in crystalline form.

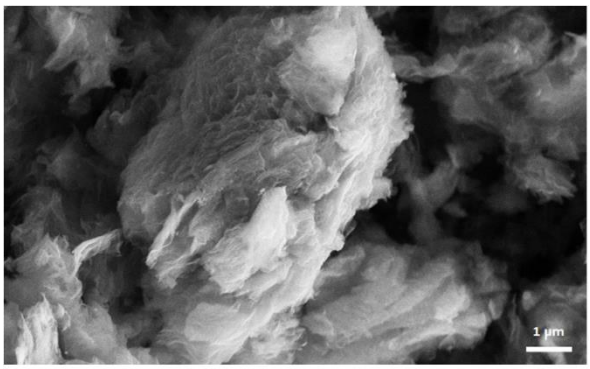

(a)

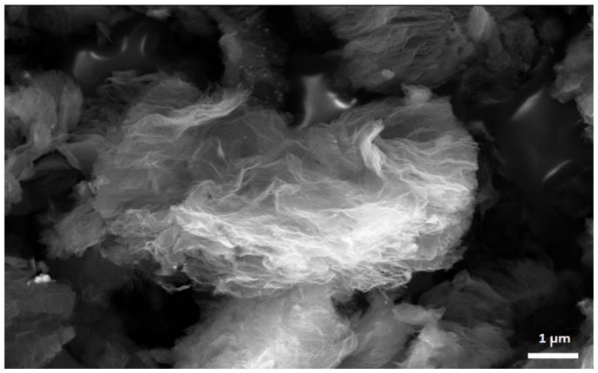

(b)

Figure 5. SEM image of the graphene flakes and information about morphology, (a) SEM images of GN and (b) GO flakes used as fillers in this work of GO agglomerated.

As can be seen in Figure 5 (a), GN presents multilayered flakes with a high degree of anisotropy and a rough structure with a few microns in diameter. The GO structures presented in Figure 5 (b) also exhibit an irregular structure, and the random ripples corresponding to the particular graphene layers are clearly visible. Oxidation of GN affects the flakes, leading to the crumpled and wrinkled structure desired for subsequent incorporation and well-dispersion into the resin matrix.

As the uniform distribution of the filler is a key parameter determining the

The presence of the groups in the GO and GO filler was before and after the incorporation into the polymer matrix was determined using Attenuated Total Reflection (ATR) technique. In the GN spectrum, presented in Figure 6 (a) bands attributed to C-H bonds at about 2920 and 2852 cm^{-1} are clearly seen [50].

10.1002/cnma.202400488

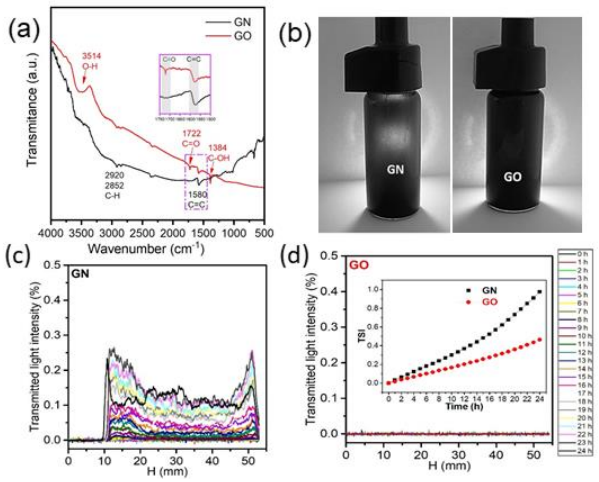

Figure 6. (a) FT-IR spectra of GN and GO, (b) photography of the sample holder used for Turbiscan analysis filled with GN and GO. Turbidimetry results for (c) GN and (d) GO. Inset shows the TSI change for both fillers.

Next, the band at about 1580 cm^{-1} can be ascribed to vibrations of C=C bonds with sp^2 hybridization [51]. The presence of C=C double bonds is typical of graphene materials [50-51], while C-H bonds with sp^3 hybridization are a residue from the process of graphene synthesis in acidic medium [52]. In GO, in addition to the aforementioned bands, additional bands are seen at 3514, 1722 and 1384 cm^{-1} that is attributed to O-H, C=O and C-OH bonds, respectively [50-51, 53]. FT-IR analysis confirms that the graphene surface was effectively oxidized, and hydroxyl and carboxyl groups were attached to the surface as a result of the oxidation process. The main purpose of graphene oxidation was to increase filler dispersion in the resin-based matrix and improve interfacial integration towards enhanced mechanical properties.

To determine the homogeneity of the carbon-based platelets, dispersion in the resin was evaluated with the turbidimetric method in which the light transmission through the sample at different height-points are measured [54]. The measurement was conducted at room temperature for 24 h, where the proposed time relates to the resin crosslinking conditions (crosslinking time indicated by the manufacturer). Figures 6(c) and 6(d) shows the destabilization of graphene dispersion in the epoxy resin, what relates to aggregation and sedimentation of the filler [55-56]. Oxidation of GN resulted in an increase in the stability of the filler dispersion, as evidenced by the lack of change in the amount of light passing through throughout the test run, see Figure 6(d) [55]. In order to better compare the dispersion stability of GN and GO in the resin, TSI was determined (the higher its value, the less stable the system) [57-58]. The analysis performed (inset in Figure 6(d)) showed a significant decrease in TSI values in systems with GO. The same observations were confirmed using digital photography taken after 24 h (Figure 6(a, b)) of the prepared dispersions, it can be seen that the dispersion with GO (Figure 6(b)) was not transmitted to light, indicating it higher stability compared to the system with GN. As the crosslinking takes 24 h, the stability at this time is sufficient to obtain a homogenous structure of resin-based nanocomposite with GO filler. Improving the homogeneity of systems with GO may increase the interfacial interaction and improve the mechanical properties of nanocomposites with its participation.

The XRD pattern obtained from the commercial graphene powder showed that the material is condensed into a graphite-like structure presented in the literature [71] with a characteristic set of Bragg peaks, marked in Figure 7 (a, b) by the corresponding Miller indices. The predominance of the intensities of the (00l) Bragg peaks naturally indicates the crystalline orientation of the larger surface of the flakes in the sample. On the other hand, the XRD pattern obtained for the oxidized sample shows the same structure, but the width of the Bragg peaks increases by more than 2.5 times, indicating a decrease in the average crystallite size that can be ascribed to the oxidation of GN in highly acidic media that could also etch the surface leading to its size reduction. The pattern recorded for the nanocomposite confirm the incorporation of the GN and GO into the polymer structure complementary to the abovementioned FTIR-based analysis.

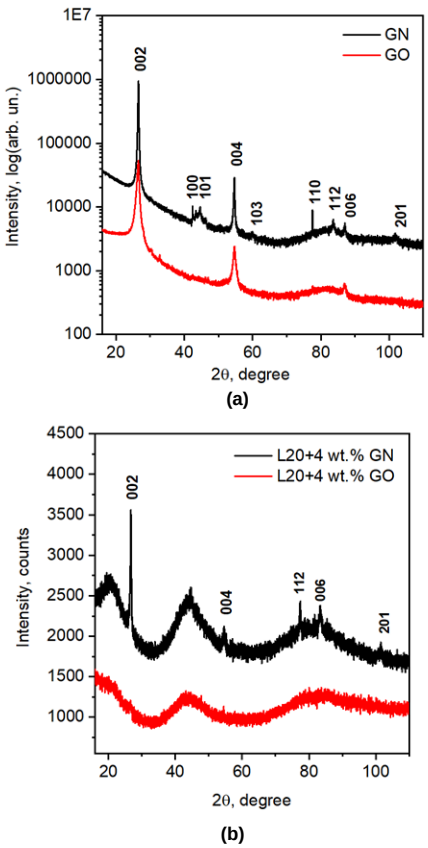

Figure 7. XRD pattern of (a) GN (black solid line) and GO (red solid line) materials, and (b) GN and GN in the epoxy resin matrix.

Thermal expansion tests

The following test was focused on the determination of the thermal expansion and the glass transition temperature of the nanocomposite. As can be seen in Figure 2 and Table 1, the glass transition temperature T_g increases for the GN-based nanocomposite at low filler content (0.1 wt.%), what can be related to the good dispersion of GN in the resin matrix.

Table 1. Thermal expansion analysis results.

Material	Heating cycle			Cooling cycle		
	T_g (°C)	CTE I 25-80°C (μm/m°C)	CTE II 125-180°C (μm/m°C)	T_g (°C)	CTE I 25-80°C (μm/m°C)	CTE II 125-180°C (μm/m°C)
EP L20 neat	100.9	73.4	181.4	94.3	74.3	187.9
EP L20+0.1 wt.% GN	105.2	69.9	188.0	97.9	73.2	192.0
EP L20+0.5 wt.% GN	101.3	72.4	185.9	95.6	74.1	188.9
EP L20+1 wt.% GN	101.2	72.8	184.9	96.2	74.9	188.2
EP L20+2 wt.% GN	105.8	68.2	183.4	98.0	74.3	187.9
EP L20+4 wt.% GN	112.2	68,9	171.8	104.1	69.1	178.3
EP L20+0. wt.%1 GO	101.1	72.1	188.6	96.2	74.1	189.7
EP L20+0.5 wt.% GO	109.7	66.3	180.2	103.0	69.9	184.1
EP L20+1 wt.% GO	109.8	66.2	178.9	103.3	69.5	183.4
EP L20+2 wt.% GO	109	64.4	174.2	104.2	68.2	180.7
EP L20+4 wt.% GO	115	64.2	172.7	105.8	68.0	179.2

Well-dispersed GN can cause stiffening of the structure and limit mobility of polymer chain segments or increase crosslinking consequently leading to the increase in T_g [59, 60]. However, the increase of GN content results in higher T_g values comparing to Epoxy/0.1 wt.% GN what can be caused by the filler agglomeration. Only relatively high shares of GN (4 wt.%) caused an increase in the value of the measured parameter compared to materials containing 0.1 wt.% GN. Materials obtained with GO were characterized by significantly higher values of T_g at higher than 0.1 wt.% GO share of this filler in the resin. In addition, no decrease in T_g values of these materials was observed with an increase in the proportion of GO. This indicates better dispersion of GO in the nanocomposites and improved interfacial interaction due to the introduction of additional functional groups on the graphene surface after the oxidation process [6, 61].

As the thermal expansion coefficient describes changes in material length as a function of temperature, it is an important parameter for epoxy resin for its potential application as the reinforcement material. Analysis of this parameter in the temperature range below T_g in the heating cycle indicated an initial value decrease of CTE. Then, this value increased at higher GN content (0.5 wt.%, 1 wt.%) to decrease again in materials containing 2 wt.%. and 4 wt.% fillers. In contrast, results from the cooling cycle indicated little change in the expansion coefficient of materials containing less than 4 wt.% of graphene. Nanocomposites with GO were characterized by a decrease in the linear expansion coefficient as the filler percentage increased. Analysis of the coefficient of thermal expansion above the glass transition temperature of the obtained graphene-filled nanocomposites showed, only in the case of Epoxy/4 wt.% GN, its significant reduction compared to neat Epoxy L20. Despite a gradual decrease in CTE with an increase of GN content in the resin matrix, a higher expansion coefficient compared to the unmodified matrix material was observed. This trend was observed in both heating and cooling cycles. For GO nanocomposites, a significant reduction in CTE values were recorded up to 0.5 wt.% of GO filler.

As the GN materials have a very low coefficient of thermal expansion [62-63] its incorporation into an epoxy resin can lower its CTE. However, the key parameters affecting the mobility limitation of polymer chain segments and consequently the expansion coefficient are the homogeneity of the filler dispersion and the high degree of filler-polymer interfacial interactions [5, 64] where the introduction of additional functional groups can increase their interactions [65]. Therefore, GO, which dispersed more effectively in the epoxy resin matrix, caused lowering of α below T_g at lower filler content. In addition, the presence of functional groups on the surface of GO improves the dispersion in the resin matrix resulting in lowering the coefficient of thermal expansion of Epoxy/GO nanocomposites also above T_g (where the segments of the polymer chain gain greater mobility) even at relatively low filler shares.

Mechanical properties studies

Selected mechanical properties results of neat epoxy resin and EP L20 GN and EP L20 GO filled 0.1, 0.5, 1.0, 2.0, 4 wt.%

graphene flakes and oxidized graphene flakes composites are shown in Table 2.

Table 2. Selected mechanical properties of EP L20 unfilled, EP L20 filled GN and L20 filled GO.

Material	Density (g/cm3)	Young's modulus nanoindentation (GPa)	Hardness (GPa)
EP L20 neat	1.1935 (±0.0038)	4.04 (±0.05)	0.222(±0.003)
EP L20+0.1 wt.% GN	1.1870 (±0.0056)	3.72 (±0.03)	0.223(±0.004)
EP L20+0.5 wt.% GN	1.1804 (±0.0049)	4.15 (±0.09)	0.238(±0.006)
EP L20+1 wt.% GN	1.1794 (±0.0033)	3.90 (±0.14)	0.225(±0.013)
EP L20+2 wt.% GN	1.1908 (±0.0038)	3.90 (±0.12)	0.220(±0.042)
EP L20+4 wt.% GN	1.1996 (±0.0053)	5.25 (±0.15)	0.212(±0.018)
EP L20+0.1 wt.% GO	1.1813 (±0.0026)	3.80 (±0.11)	0.217(±0.007)
EP L20+0.5 wt.% GO	1.2010 (±0.0026)	3.80 (±0.13)	0.219(±0.012)
EP L20+1 wt.% GO	1.2144 (±0.0036)	4.25 (±0.13)	0.217(±0.006)
EP L20+2 wt.% GO	1.2058 (±0.0012)	4.32 (±0.15)	0.242(±0.008)
EP L20+4 wt.% GO	1.2080 (±0.0036)	5.60 (±0.25)	0.218(±0.028)

In brackets measurement uncertainty, EP L20+wt.% GN - it means epoxy with graphene fillers, EP L20+wt.% GO- it means epoxy with oxidate graphene fillers.

To obtain statistically necessary results, a minimum of three specimens per state was used. Young's modulus by nanoindentation [66-68] is vary due to differences in sample composition. The measurement uncertainty is given in brackets of Table 2. Elastic modulus measured with a Berkovich pyramidal indenter increased significantly for EP L20 GO 1, 2, and 4 wt.% doped flakes due to the formation of the inter-connecting graphene network. Our tested nano-reinforced polymer-based nanocomposite evidenced the fact that macroscopic properties depend on the weight fraction of the heterogeneous inclusion at the nanoscale.

During experiments the displacement and strain distributions were obtained from the visible range (0.3 - 1 μm) image sequence using a Manta G-125B charge-coupled device (CCD) camera and a digital image correlation algorithm software developed in IPPT PAN by Nowak and Maj (2018) [69]. The average global strain obtained by DIC, was calculated by dividing the displacement between the upper and lower edges of the gauge region (measured using DIC) and dividing it by the original gauge region length. The results show that all toughened up EP L20 GO resin can carry higher stresses than the toughened EP L20 GN resin. In tension and compression, a ductile response is observed at quasi-static strain rate ($\dot{\varepsilon}$ = 0.001 s^{-1}). The axial component of the nominal stress in tensile tests causes early failure in the EP L20 GN 4 wt.% and EP L20 GO 4 wt.% polymer-based nanocomposite. Observation of sample geometry during tension tests at quasi-static constant elongation rate shows no necking and no crazing in all EP L20 GN and EP L20 GO a composites.

Tension tests

An experimental study under quasi-static tensile loading conditions was conducted to detect the strength of EP L20 enriched with embedded carbon graphene and graphene oxidized nanoflakes.

Tension specimens were cut from 2 mm thick plate for the testing of nanomaterials available in the form of thin dog bone shape. The specimen dimensions are shown in Figure 3 (a) and represent a compromise between, on the one hand, a large radius of curvature in the shoulders and a relatively long parallel gauge length, to minimize stress concentrations and, on the other hand, a short overall length to allow an early attainment of quasi-static equilibrium. The specimen end tabs were clamp into parallel-sided slots in the loading bars of the MTS testing machine used for the quasi-static strain rate tests. The displacement measured between the adjacent ends of the loading bars was assumed to be concentrated over a central 6 mm gauge region of the tensile specimen. In all the MTS machine tests, strain gauges attached to the specimen, had gave the axial strains which agreed well with those determined by DIC methods in this area.

Figure 8 (a) shows the mean stress-strain response for nominally identical tests on EP L20 neat epoxy resin and epoxy filled GN nanoflakes while Figure 8 (b) shows the mean stress-strain response for neat epoxy resin and epoxy resin filled GO nanoflakes during the uniaxial tension process for quasi-static strain rates $\dot{\varepsilon}$ = 0.001 s^{-1}. As seen, tensile properties show an upward trend with the addition of GO and reach the highest point at 0.5 wt.% of GO.

10.1002/cnma.202400488

RESEARCH ARTICLE

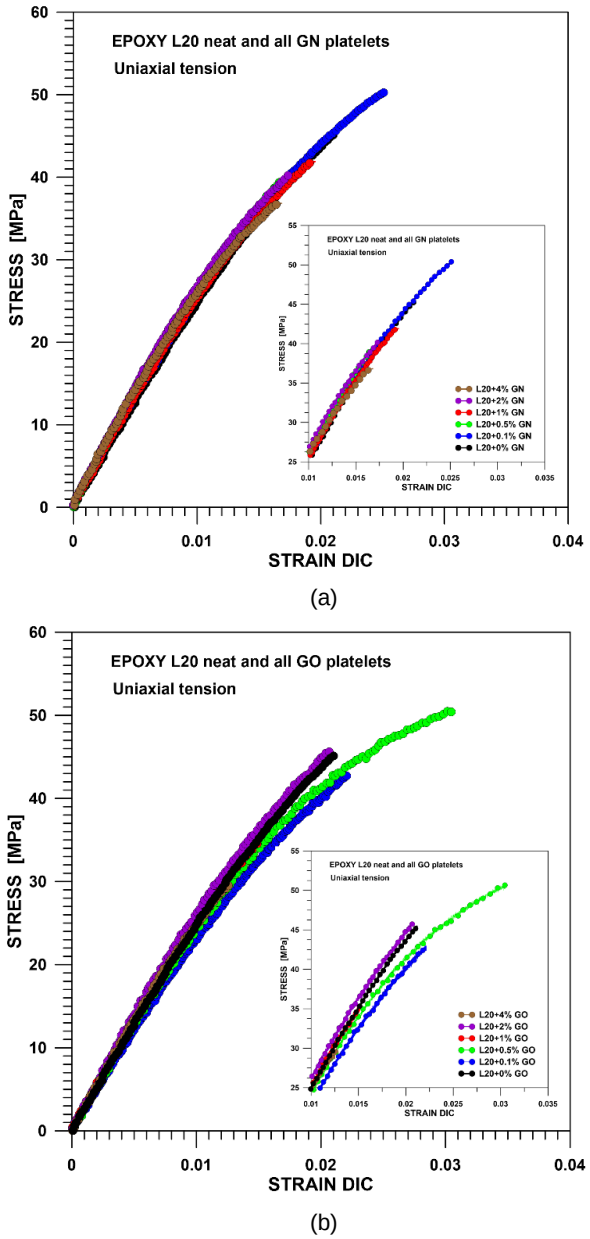

Figure 8. Stress-strain response of (a) L20 epoxy resin filled GN flakes and (b) epoxy resin filled GO flakes during the uniaxial tension process for quasi-static strain rates.

With results obtained by DIC method through conducted and presented tests, the evolution of the strain fields components distribution maps for EP L20 2 wt.% GO sample for a nominal strain, as representative for increase inelastic deformation, are presented in Figure 9 (a, b, c), Figure 10 (a, b, c) and Figure 11 (a, b, c). All maps were presented in the same way in progress for following nominal strains e = 0.001, 0.01, and 0.02. The interpretation of strains is depending on the coordinate system, for tensile specimen the axis direction of applied coordinate system are shown in Figure 3 (a). The strain field in the transverse ε_{xx} direction is reported in Figure 9 (a) for a nominal strain of e=0.001 for specimen EP L20 2 wt.% GO.

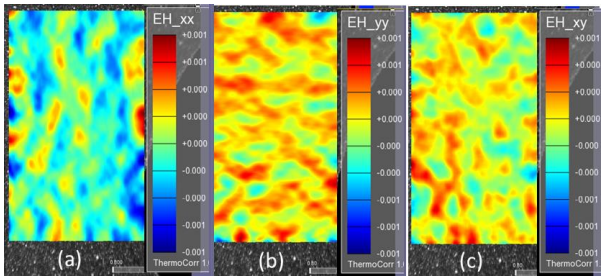

Figure 9. The distributions of logarithmic strain fields for the transverse ε_{xx} axial ε_{yy} and shear ε_{xy} components during the uniaxial tension process for quasi-static strain rates. The field plots correspond to a nominal strain of e = 0.001.

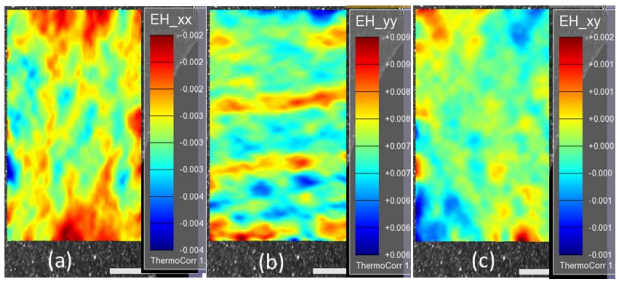

Figure 10. The distributions of logarithmic strain fields for the transverse ε_{xx}, axial ε_{yy} and shear ε_{xy} components during the uniaxial tension process for quasi-static strain rates. The field plots correspond to a nominal strain of e = 0.01.

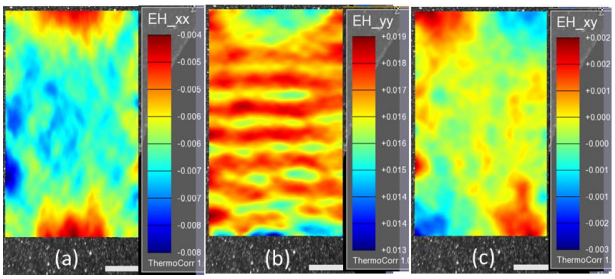

Figure 11. The distributions of logarithmic strain fields for the transverse ε_{xx}, axial ε_{yy} and shear ε_{xy} components during the uniaxial tension process for quasi-static strain rates. The field plots correspond to a nominal strain of e = 0.02.

The strains are scattered throughout the surface and the values are so closely matched. In tension the axial displacement increasing evenly as the load increased. However, the strain field in the longitudinal ε_{yy} direction obtained for testing specimen EP L20 2 wt.% GO are nonhomogeneous and is reported in Figure 9 (b) for the same a nominal strain of e = 0.001 like in Figure 9 (a). The initiation of the effect of weave pattern on the strain field can be seen in Figure 9 (b), but this effect of the weave on the strain field in the tension direction is not yet distinct. The strain field of the ε_{xy} similarly to ε_{xx} is also evenly distributed and can be seen in Figure 9 (c).

For more advanced stage of the deformation with nominal strain of e=0.01 for specimen EP L20 2 wt.% GO, the tensile strain field in the transverse ε_{xx} direction is reported in Figure 10 (a). The strains ε_{xx} with maximum value represented by red color in the middle of top and bottom edges considerably increase. The strain field in the longitudinal ε_{yy} direction, obtained while testing

specimen EP L20 2 wt.% GO, is reported in Figure 10 (b) for a nominal strain of e=0.01. The effect of the weave pattern on the strain field ε_{yy} is also visible in Figure 10 (b), but the effect of the weave is more emphasized. In Figure 9 (c) the values of strain ε_{xy} start to increase in left top and right bottom corners.

Consider the deformation for a nominal strain of e=0.02 the strain field in the transverse ε_{xx} direction is reported in Figure 11 (a) for specimen EP L20 2 wt.% GO. The strains ε_{xx} decrease in center regions, but the strains are more intensively localized in center of top and bottom region of sample. The strain field in the longitudinal ε_{yy} direction, obtained while testing specimen EP L20 2 wt.% GO is reported in Figure 11 (b) for the same a nominal strain of e = 0.02. Again the effect of the weave pattern on the strain field ε_{yy} can also be seen in Figure 11 (b). Furthermore, the effect of the weave on the strain field in the longitudinal direction ε_{yy} is more significant. The shear strain field ε_{xy} for a nominal strain of e = 0.02 still increase and can also be seen in Figure 11 (c), and more intensive strains are developed into top left and into bottom right corners of sample.

The repeatability of the tension tests showed much more variability. Specimens broke in an apparently random manner in the middle of the gauge section or at the transition between the parallel gauge section and the tab, giving very different results as illustrated in Figure 8 (a, b) for quasi-static tests. The brittleness of all EP L20 GN and EP L20 GO materials, indicated by the strain at break attributed to fractures in Figure 8 (a, b), is a contributory factor to the scatter of the results in tension. Although considerable care was taken to ensure axial setting of the test piece, the bending stresses introduced by even minor misalignment in sample could cause too early failure. Even if a perfectly uniform state of tension were to be achieved, scatter would still arise, since existing microvoids. In the final specimen's analysis just immediately after tensile tests reveals that the mode of failure in tension can be identified explicitly as the brittle fracture for EP L20 GN and EP L20 GO specimens of the present study. In Figures 8 (a, b) the initial tension modulus, the maximum stress reached and the corresponding tensile strain, offers a representation of behavior of enrich epoxy-resin. For each enriched EP L20 nanocomposite with embedded carbon graphene nanoflakes there is an increase in modulus and different maximum stress for corresponding strain under low strain rate loading, the maximum stress effects being most marked for the epoxy resin with 0.1 wt.% GN and 0.5 wt.% GO specimens. The general trends illustrated in Figures 8 (a, b) are reproducible and allow a qualitative ranking of tested materials.

Compression tests

The specimen for compression tests is a cylinder defined by its aspect ratio L/D=1.56 and is compressed between two flat-ended steel plates. Quasi-static uniaxial compression tests were conducted on the MTS 585 Mini Bionix II electric mechanical universal testing machine under displacement controlled uniaxial compression at room temperature (298 K). All tests were reproduced minimum three times to guarantee accuracy. Experiments were successfully performed on formulations of epoxy matrix and with varying GN and GO flakes at quasi-static strain rates $\dot{\varepsilon}$ = 0.001 s^{-1}. A mean stress-strain plots for neat EP L20, EP L20 GN and EP L20 GO at quasi-static strain rate are shown in Figure 12 and Figure 13.

These figures clearly show the dependence of yield strength on the graphene dopant as well as the strain softening and hardening effect. This is representative of the trend displayed by all tested materials. The friction between the specimen and the loading bars has not been taken into account when investigating the strain of tested nanocomposite over a strain rate range of 10^{-3} s^{-1}. Mean stress-strain curves for three nominally identical tests on EP L20 GN specimens are presented in Figure 12 and demonstrate that the results are extremely repeatable. In this graph, and all others presenting results in terms of true stress and true strain, incompressibility was assumed, and the maximum volumetric strain in these tests being estimated at only 2 wt.%. Mean quasi-static stress-strain curves for the EP L20 GO resin are reported in Figure 13. The stress-strain curves have a very similar shape but the gradients in the strain stiffening region vary slightly. As the strain on the specimen increased, the specimen showed cracks on the surfaces aligned in vertical directions.

10.1002/cnma.202400488

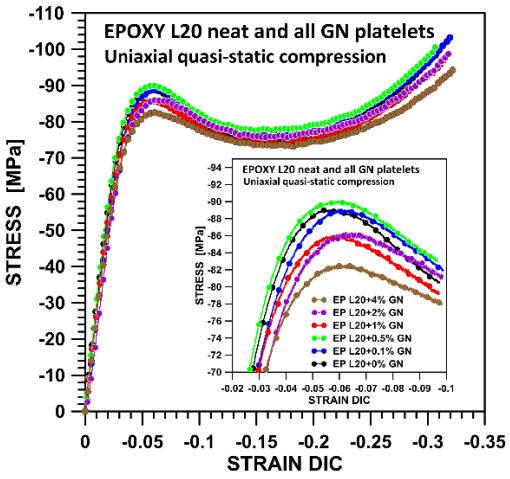

Figure 12. Stress-strain response of EP L20 resin filled with weight fractions graphene flakes: 0.1, 0.5, 1, 2 and 4 wt.% GN at quasi-static strain rates shows typical post yield softening, and strain hardening.

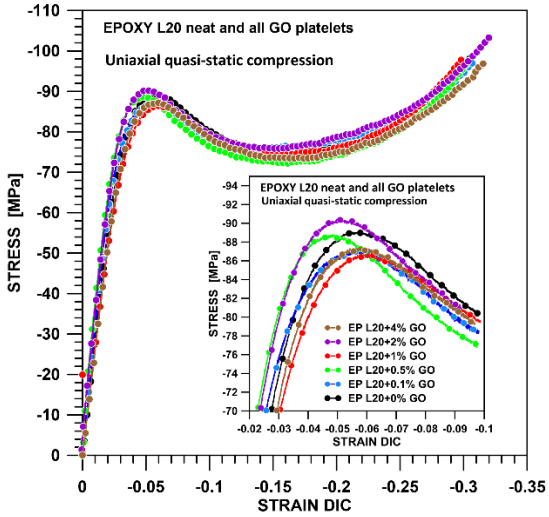

Figure 13. Stress-strain response of EP L20 resin filled with weight fractions graphene oxidized flakes: 0.1, 0.5, 1, 2 and 4 wt.% GO at quasi-static strain rates shows typical post yield softening, and strain hardening.

Results and analysis

This section discusses the impact of 0.1, 0.5, 1, 2, 4 wt.% of GN and GO nanoparticles on the strength of an epoxy nanocomposite.

The mean stress-strain response of the EP L20 nanocomposite under uniaxial compression loading at room temperature and strain rate 0.001 s^{-1} is shown in Figure 12 and Figure 13. The material exhibits following mechanical characteristics: initial elasticity, yielding, strain softening and strain hardening. The first observation is that for quasi-static strain rates compression tests, specimens deform in a ductile manner up to a strain of 0.30. In these tests, the stress-strain responses are similar and stress-strain curves are smooth.

The correlation between the displacements measured with mechanical gauges and with DIC was highly satisfactory. DIC can capture multi-direction field strains of regions which are smaller than common strain gauges. In tension tests the consistent measurement results showed the opportunity for measuring and observing the fracture strains of EP L20 GN and GO nanocomposites materials and capture how the stresses are influenced by these strains. The results of tension tests obtained with DIC (Figures 9-11) gave insight on how the strains were distributed on sample surface, and how the strains in the transverse direction had an effect on the strain localization was expected. Additionally, DIC helped detecting anomalies in some tests that would have otherwise ignored the results from traditional equipment.

Tensile strength

A stress-strain response of graphene-resin nanocomposite subjected to monotonic loading at room temperature exhibits in case of tension increase in the stress until fracture. Figures 8 (a, b) illustrate the tensile stress-strain curves for L20 epoxy resin filled GN and GO nanoflakes and epoxy neat resin during the uniaxial tension process for quasi-static strain rates $\dot{\varepsilon}$ = 0.001 s^{-1}, respectively. In Figure 14 (a, b) the ultimate tensile strength values for EP L20 GN and EP L20 GO nanocomposites are presented.

The tensile strength of filled epoxy-resins is between 37 and 50 MPa for EP L20 GN and between 30 and 51 MPa for EP L20 GO at quasi-static strain rate. For EP L20 GO nanocomposites the increased tensile strength can be attributed to the oxidation on the GN particles surfaces, which gave them the crumpled and wrinkled structure (TEM micrographs in Figure 5) and promoted interlocking and restriction of the epoxy resin chains against mobility on the application of load. However, increase in L20 GO concentration of flakes to 4 wt.% reduced the tensile strength to about 30 MPa. The reduction of strength can be attribute to the unavoidable formation of nanoparticles clusters in the epoxy matrix as its content increased, which result in more nanoparticles interactions than nanoparticles to matrix interactions. This leads to poor load transfer from the matrix to the nanoparticles due to reduction in adhesion between the nanocomposites components.

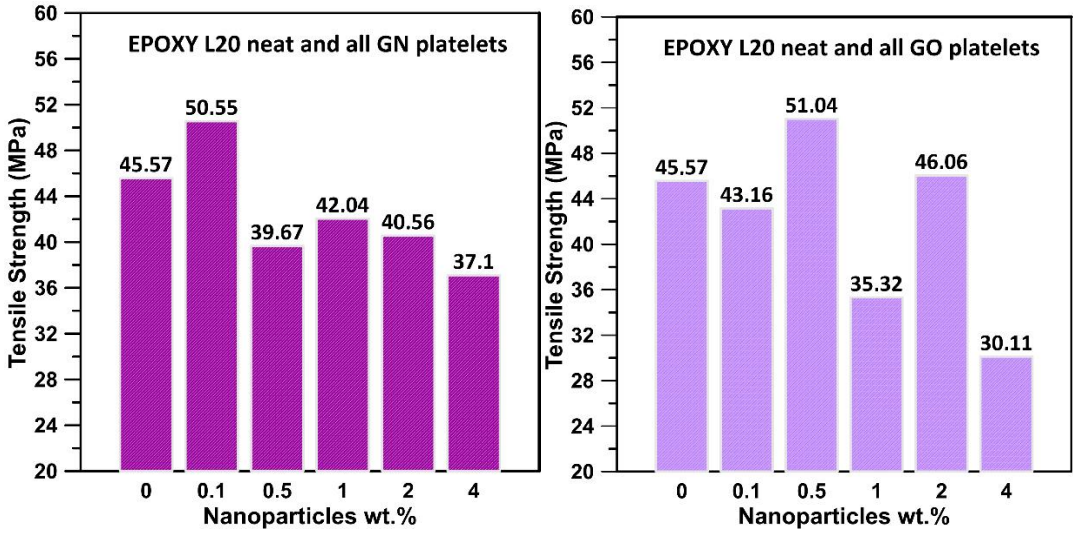

Figure 14. Tensile strength of the nanocomposite with different nanoparticle weight percentages (a) L20 epoxy resin filled GN flakes and (b) epoxy resin filled GO flakes during the uniaxial tension process for quasi-static strain rates.

Hardness

The nanoindentation hardness values obtained for the unfilled epoxy and its nanocomposites are summarized in Table 2. Graphically, the change in hardness with reference to the percentage of additives blended with epoxy resin matrix is shown in Figure 15(a, b). From the Table 2 and in Figure 15 (a, b), it is inferred that the neat epoxy displays its hardness as 0.222 GPa while a maximum the hardness values found of 0.238 GPa is noticed for a composite EP L20 GN having 0.5 wt.% GN (in Table 2 EP L20+0.5% GN). In the case of all EP L20 GO series, the hardness values increased to a maximum of 0.242 GPa for a composite EP L20 GO having 2 wt.% (in Table 2 EP L20+2 wt.% GO) in contrast to all other compositions.

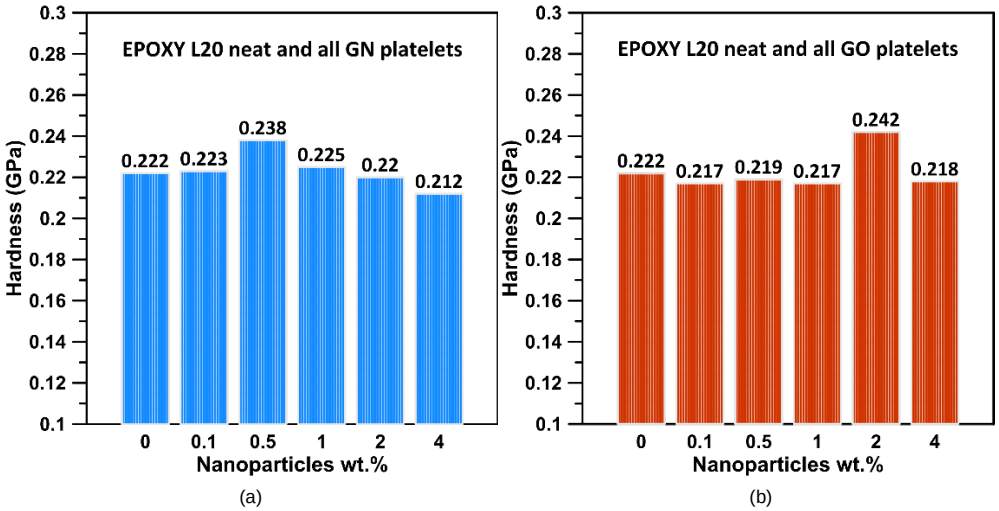

Figure 15. Hardness of the nanocomposite with different nanoparticle weight percentages (a) L20 epoxy resin filled GN flakes and (b) epoxy resin filled GO flakes during the uniaxial tension process for quasi-static strain rates.

Decomposition of stress-strain response

A stress-strain response of graphene-resin nanocomposite subjected to monotonic loading at room temperature demonstrate, in case of compression load, elastic deformations until yield followed by post yield plastic flow, and finally strain hardening at large strains (e.g. Figure 12). The overall trend of the stress-strain response for compression is similar for all type of EP L20 samples. In compression the stress-strain post yield plastic flow response can be distinguish the upper and lower yield stress, which are defined as a points $\partial\sigma/\partial\varepsilon$, (see Figure 11 and Figure 12). The upper yield stress and the lowest post yield stress for samples

with different nanoparticle weight percentages are presented in Figure 16 (a, b), respectively.

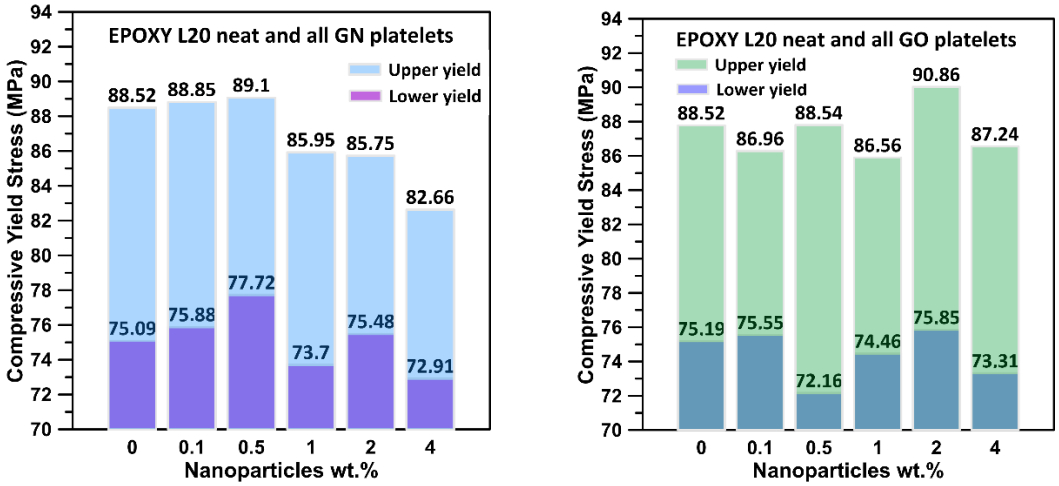

(a) (b)

Figure 16. The yield stresses of the nanocomposite with different nanoparticle weight percentages (a) L20 epoxy resin filled GN flakes and (b) epoxy resin filled GO flakes during the uniaxial compression process for quasi-static strain rates.

There is substantial change of the upper and lower yield stress. The upper yield stress is between 82 and 89 MPa for EP L20 GN and between 86 and 91 MPa for EP L20 GO at quasi-static strain rate $\dot{\varepsilon} = 0.001\ s^{-1}$.

The stress-strain response up to yield as a function of strain can be described using an elasticity model. The initial elastic slope of the stress-strain curve slightly increases with increase of the weight fraction of graphene dopant Figure 8 (a, b). However, for plastic flow response J_2 plasticity flow equations usually are used to predict the strain and stress states.

Summary and concluding remarks

This work demonstrates the incorporation of the GN-based fillers in the epoxy resin matrix with different GN and GO content over the resin volume, where the filler was uniformly dispersed into the bulk material. The main objective of this study is a comprehensive investigation of the mechanical properties of epoxy polymer nanocomposites infused with graphene-based nanoflakes, ranging from neat epoxy production to the characterization of nanoflakes and subsequent mechanical testing. However, besides the thermal and mechanical aspects of this work, the improvement of the stability of the suspension during cross-linking with the GO was studied. As the GO contains oxygen onto its structure in the functional groups, the dispersion was improved leading to the enhanced abovementioned properties. The weight fractions of up to 4 wt.% were studied, employing a thermo-mechanical analyzer, SEM and HR-TEM techniques to confirm well-defined filler morphology and their incorporations in polymer matrix. Tension and compressive tests were conducted at room temperature using a universal testing machine, and the resulting stress-strain responses, along with deformation processes monitored through Digital Image Correlation (DIC), provided valuable insights into quasi-static strain rate deformations.

The experiments revealed notable trends in the mechanical behavior of the epoxy matrix doped with graphene flakes. Tensile tests exhibited experimental scatter of the strain at break attributed to brittle fractures, yet discernible trends showed a significant increase in initial modulus and a slight rise in maximum stress. Compression tests for EP L20 GN and EP L20 GO highlighted changes in yield strength and elastic modulus with varying weight fractions of graphene nanoflakes, illustrating a consistent trend across materials.

Achieving a uniform dispersion of filler in the matrix is crucial for nanocomposites, impacting interfacial effects. Despite efforts to homogenize the distribution, unevenness may persist due to interactions such as hydrogen bonds, π-π interactions, and electrostatic forces.

The test results indicated that inclusion of graphene into nanocomposites resulted in low coefficients of thermal expansion (CTEs), and increasing graphene fraction reduced CTEs more significantly. The 4 wt.% graphene oxide-based nanocomposite shows 12.5 % reduction of CTE in heating cycle and 5 % reduction of CTE in cooling cycle below the glass transition temperature. An increase of 14 °C in the glass transition temperature was observed along with the reduction of CTE in heating cycle.

The tensile strengths show improvement with particles smaller than 1 % weight fraction, while even at a low 0.1 wt.%, inadequate dispersion and flakes agglomeration can reduce tensile stress. The compressive yield stress increased to a maximum of 90.86 MPa for the epoxy nanocomposite having 2 wt.% oxidized graphene flakes.

Recent research has intensified the exploration of particle-matrix interactions, emphasizing the need to understand these interactions at the molecular level and their effect on the physicochemical characteristics of the obtained nanocomposite. In this study, the presence of oxygen atoms on graphene flakes facilitated favorable conditions for hydrogen bonding interactions, contributing to an enhanced locally ordered structure and π-π interactions with the polymer matrix. The identified mechanical response features lay the groundwork for developing constitutive models tailored to nanocomposites enriched with the graphene.

The findings from thermal tests provide a reasonable recommendation for graphene-enabled thermal management in electronic engineering, while the mechanical studies confirm the promising properties to be used in other industrial sectors.

Conflict of Interest

The authors declare no conflict of interest.

Data availability statement

The data that support the findings of this study are available from the corresponding author upon reasonable request.

Acknowledgements

The authors acknowledge in various ways and valuable contribution to this work from late Prof. Ryszard B. Pęcherski. Sincere thanks are expressed to Mr. Leszek Urbański (IFTR PAS, Poland) for performing the mechanical investigation.

Keywords: epoxy resin; nanocomposite; carbon nanoparticles; tensile strength; compression strength; thermal stability

References

[1] X. Liang, X. Li, Y. Tang, X. Zhang, W. Wei, X. Liu, *J Colloid Interface Sci* **2022**, *611*, 105, https://doi.org/10.1016/j.jcis.2021.12.068.

[2] Y. Wei, X. Hu, Q. Jiang, Z. Sun, P. Wang, Y. Qiu, W. Liu, *Compos. Sci. Technol* **2018**, *161*, 74, https://doi.org/10.1016/j.compscitech.2018.04.007.

[3] Y. Guo, C. Bao, L. Song, B. Yuan, Y. Hu, *Ind. Eng. Chem. Res.* **2011**, *50(13)*, 7772, https://doi.org/10.1021/ie200152x.

[4] X. Wang, L. Song, W. Pornwannchai, Y. Hu, B. Kandola, *Compos. Part A Appl. Sci. Manuf* **2013**, *53*, 88, https://doi.org/10.1016/j.compositesa.2013.05.017.

[5] S. Wang, M. Tambraparni, J. Qiu, J. Tipton, D. Dean, *Macromolecules* **2009**, *42*, 5251, https://doi.org/10.1021/ma900631c.

[6] L.C. Tang, Y.J. Wan, D. Yan, Y.B. Pei, L. Zhao, Y.B. Li, L.B. Wu, J.X. Jiang, G.Q. Lai, *Carbon* **2013**, *60*, 16, https://doi.org/10.1016/j.carbon.2013.03.050.

[7] B. Tang, G. Hu, H. Gao, L. Hai, *International Journal of Heat and Mass Transfer* **2015**, *85*, 420, https://doi.org/10.1016/j.ijheatmasstransfer.2015.01.141.

[8] T. Kuilla, S. Bhadra, D. Yao, N.H. Kim, S. Bose, J.H. Lee, *Progress in Polymer Science* **2010**, *35(11)*, 1350, https://doi.org/10.1016/j.progpolymsci.2010.07.005.

[9] J.R. Potts, D.R. Dreyer, Ch.W. Bielawski, R.S. Ruo_, *Polymer* **2011**, *52*, 5, https://doi.org/10.1016/j.polymer.2010.11.042.

[10] J.A. King, D.R. Klimek, I. Miskioglu, G.M. Odegard, *J. Appl. Polym. Sci*. **2013**, *128*, 4217, https://doi.org/10.1002/app.38645.

[11] Z. Zhang, W. Zhang, D. Li, Y. Sun, Z. Wang, C. Hou, L. Chen, Y. Cao, Y. Liu, Int. J. Mol. Sci. **2015**, *16(1)*, 2239, https://pubmed.ncbi.nlm.nih.gov/25608656.

[12] J. Guest, I.A. Kinloch, R.J. Young, *J Mater Sci* **2023**, *58*, 9473, https://doi.org/10.1007/s10853-023- 08603-3.

[13] G. Yang, L. Li, W.B. Lee, M. Ng, *Science and Technology of Advanced Materials* **2018**, *19(1)*, 613, https://doi.org/10.1080/14686996.2018.1494493.

[14] V.B. Mohan, K. Lau, D. Hui, D. Bhattacharyya, *Compos. Part B Eng* **2018**, *142*, 200, https://doi.org/10.1016/j.compositesb.2018.01.013.

[15] N.P. Singh, V.K. Gupta, A.P. Singh, *Polymer* **2019**, *180*, 121724, https://doi.org/10.1016/j.polymer.2019.121724.

[16] C. Shen, S.O. Oyadiji, *Materials Today Physics* **2020**, *15*, 100257, https://doi.org/10.1016/j.mtphys.2020.100257

[17] M.K. Shukla, K. Sharma, *Polym. Sci. Ser. A* **2019**, *61*, 439, https://doi.org/10.1134/S0965545X19040096.

[18] A. Alipour, R. Lin, K. Jayaraman, *J Mater Res Technol* **2021**, *15,* 4610, https://doi.org/10.1016/j.jmrt.2021.10.082.

[19] L. Shan, C.Y. Tan, X. Shen, S. Ramesh, M.S. Zarei, R. Kolahchi, M.H. Hajmohammad, *J Mater Res Technol* **2023**, *24*, 7570, https://doi.org/10.1016/j.jmrt.2023.04.267.

[20] J.S. Jayan, A. Saritha, B.D.S. Deeraj, K. Joseph, *Mater. Chem. Phys* **2020**, *248*, 122930, https://doi.org/10.1016/j.matchemphys.2020.122930.

[21] P. Govindaraj, A. Sokolova, N. Salim, S. Juodkazis, F.K. Fuss, B. Fox, N. Hameed, *Compos. Part B Eng* **2021**, *226,* 109353, https://doi.org/10.1016/j.compositesb.2021.109353.

[22] H.M. Chong, S.J. Hinder, A.C. Taylor, *J Mater Sci* **2016**, *51*, 8764, https://doi.org/10.1007/s10853-016- 0160-9.

[23] F.A.M.M. Gonçalves, M. Santos, T. Cernadas, P. Alves, P. Ferreira, *J Mater Sci* **2022**, *57*, 15183, https://doi.org/10.1007/s10853-022-07573-2.

[24] L.B.T. La, H. Nguyen, L.Ch. Tran, X. Su, Q. Meng, H.-Ch. Kuan, J. Ma, *Advanced Nanocomposites* **2024**, *1(1)*, 39, https://doi.org/10.1016/j.adna.2023.10.001.

[25] S.A. Shojaee, A. Zandiatashbar, N. Koratkar, D.A. Lucca, *Carbon* **2013**, *62*, 510, https://doi.org/10.1016/j.carbon.2013.05.068.

[26] Z. Li, L. Deng, I.A. Kinloch, R.J. Young, *Prog. Mater. Sci* **2023**, *135*, 101089, https://doi.org/10.1016/j.pmatsci.2023.101089.

[27] A. Mostovoy, A. Shcherbakov, A. Yakovlev, S. Arzamastsev, M. Lopukhova, *Polymers (Basel)* **2022**, *14(2)*, 338, https://doi.org/10.3390/polym14020338.

[28] S.I. Abdullah, M.N.M. Ansari, *HBRC Journal* **2015**, *11(2)*, 151, https://doi.org/10.1016/j.hbrcj.2014.06.001.

[29] Y. Du, Z. Zhang, D. Wang, L. Zhang, J. Cui, Y. Chen, M. Wu, R. Kang, Y. Lu, J. Yu, N. Jiang, *Friction* **2022**, *10,* 854, https://doi.org/10.1007/s40544-021-0496-2.

[30] Z. Ren, S. Hao, Y. Xing, C. Yang, S. Dai, *Hangkong Cailiao Xuebao/Journal of Aeronautical Materials* **2019**, *39(2)*, 25, doi: 10.11868/j.issn.1005-5053.2018.000142.

[31] R. Umer, Y. Li, Y. Dong, H.J. Haroosh, K. Liao, *Int J Adv Manuf Technol* **2015**, *81(9)*, 2183, https://doi.org/10.1007/s00170-015-742.

[32] Y.J. Wan, L.Ch. Tang, L.X. Gong, D. Yan, Y.B. Li, L.B. Wu, J.X. Jiang, G.Q. Lai, *Carbon* **2014**, *69*, 467, https://doi.org/10.1016/j.carbon.2013.12.050.

[33] W. Guo, G. Chen, *J Appl Polym Sci* **2014**, *131(15)*, 1, https://doi.org/10.1002/app.40565.

[34] S.Wang, M. Tambraparni, J. Qiu, J. Tipton, D. Dean, *Macromolecules* **2009**, *42(14)*, 5251, https://doi.org/10.1021/ma900631c.

[35] L. Guo, Z. Chen, H. Han, G. Liu, M. Luo, N. Cui, H. Dong, M.-Z. Li, *Appl Nanosci* **2020**, *13*, 3273, https://doi.org/10.1007/s13204-022-02653-w.

[36] A. Garg, S. Basu, R. Mehta, R.L. Mahajan, *Polym. Compos* **2024**, *45(3)*, 2444, https://doi.org/10.1002/pc.27931.

[37] Z. Zhang, Y. Du, C. Zhu, L. Guo, Y. Lu, J. Yu, I.P. Parkin, J. Zhao, D. Guo, *Nanoscale* **2021**, *13*, 2855, http://dx.doi.org/10.1039/D0NR08600B.

[38] M. Barakat, H. Reda, A. Chazirakis, V. Harmandaris, *Polymer* **2023**, *286*, 126379, https://doi.org/10.1016/j.polymer.2023.126379.

[39] X. Yang, F. Meng, X. Zhang, B. Cao, Y. Fu, *Int. J. Therm. Sci* **2022**, *172*, 107273, https://doi.org/10.1016/j.ijthermalsci.2021.107273.

[40] U. Caliskan, H. Gulsen, *International Journal of Solids and Structures* **2023**, 285, 112553, https://doi.org/10.1016/j.ijsolstr.2023.112553.

[41] M. Pang, Y. Wang, T. Shi, Y. Jing, X. Zhang, Y. Zhang, *Compos. Struct* **2023**, *325*, 117588,https://doi.org/10.1016/j.compstruct.2023.117588.

[42] L. Lin, Y. Wang, Z. Lin, W. Luo, H. Zhang, G. Chen, H. Cao, C. Yuan, Y. Xu, B. Zeng, L. Dai, *Polymer* **2022**, *250*, 124879, https://doi.org/10.1016/j.polymer.2022.124879.

[43] H. Al Mahmud, M.S. Radue, W.A. Pisani, G.M. Odegard, *Nanomaterials (Basel)* **2021**, *2021(11)*, 2919, https://doi.org/10.3390/nano11112919.

[44] M. Yang, L. Cao, P. Yang, J. Jiang, W. Sun, Y. Li, W. Li, *Compos. Part B Eng* **2024**, *270*, 111143, https://doi.org/10.1016/j.ijthermalsci.2021.10727.

[45] H. Mehdipour, A.R. Bastami, M.H. Soorgee, *Composite Structures* **2024**, *330*, 117823, https://doi.org/10.1016/j.compstruct.2023.117823.

[46] S. Hatamie, O. Akhavan, S.K. Sadrnezhaad, M.M. Ahadian, M.M. Shirolkar, H.Q. Wang, *Materials Science and Engineering: C* **2015**, *55*, 482, https://doi.org/10.1016/j.msec.2015.05.077.

[47] Z.B. Wei, Y. Zhao, C. Wang, S. Kuga, Y. Huang, M. Wu, *Chinese J. Polym. Sci.* **2018**, *36*, 1361, https://doi.org/10.1007/s10118-018-2160-5.

[48] J. Ma, J. Liu, W. Zhu, W. Qin, *Colloids and Surfaces A: Physicochemical and Engineering Aspects* **2018**, *538*, 79, https://doi.org/10.1016/j.colsurfa.2017.10.071.

[49] H. Akhina, M.R. Gopinathan Nair, N. Kalarikkal, K.P. Pramoda, T. H. Ru, L. Kailas, S. Thomas, *Polym. Eng. Sci.* **2018**, *58(S1)*, E104, https://doi.org/10.1002/pen.24711.

[50] N. Sudesh, N. Kumar, S. Das, Ch. Bernhard, G.D. Varma, *Supercond. Sci. Technol.* **2013**, *26*, 1, https://core.ac.uk/download/pdf/20662146.pdf.

[51] Y. Altinay, E. Gökoglan, Ç. Yener, G. Ünlü, B. Sahin, *Appl. Phys. A Mater. Sci. Process* **2022**, *128*, 1, https://doi.org/10.1007/s00339-022-05929-8.

[52] M. Aziz, F.S.A. Halim, J. Jaafar, *J. Teknol.* **2014**, *69(9)*, 11, https://doi.org/10.11113/jt.v69.3388.

[53] Z. Çiplak, N. Yildiz, A. Çalimli, *Fullerenes, Nanotubes and Carbon Nanostructures* **2015**, *23(4)*, 361, https://doi.org/10.1080/1536383X.2014.894025.

[54] J. Dai, G. Wang, L. Ma, C. Wu, *J. Mater. Sci.* **2015**, *50*, 3895, https://doi.org/10.1007/s10853-015-8934-z.

[55] H. Yang, W. Kang, Y. Yu, X. Yin, P.Wang, X. Zhang, *Powder Technol.* **2017**, *315*, 477, https://doi.org/10.1016/j.powtec.2017.04.001.

[56] K.H. Nam, K. Kim, S.G. Kim, H.S. Lee, H. Jung, J. Yu, S.G. Jang, B.C. Ku, B. Moon, N.H. You, *Compos. Part B Eng* **2019**, *176*, 107236, https://doi.org/10.1016/j.compositesb.2019.107236.

[57] T.P. Nguyen and S. Wilczewski and J. Lewandowski and A. Majkowska-Pilip and K. Żelechowska- Matysiak and D. Nieciecka and W. Studziński and S.J. Olusegun and M. Syczewski and M. Giersig and T.M.T. Dinh and P. Krysiński and M. Osial, *Ceram. Int.* **2023**, *49(15)*, 25775, https://doi.org/10.1016/j.ceramint.2023.05.123.

[58] S. Perumal, A. Raji, I.W. Cheong, *Langmuir* **2018**, *34(23)*, 6737, https://doi.org/10.1021/acs.langmuir.8b00975.

[59] J.W. Yu, J. Jung, YM. Choi, J.H. Choi, J. Yu, J.K. Lee, N.H. You, M. Goh, *Polym. Chem.* **2016**, *7*, 36, http://dx.doi.org/10.1039/C5PY01483B.

[60] H. Ribeiro, W. Silva, M.T.F. Rodrigues, J.C. Neves, R. Paniago, C. Fantini, H.D.R. Calado, L.M. Seara, G.G. Silva, *J. Mater. Sci.* **2013**, *48*, 7883, https://doi.org/10.1007/s10853-013-7478-3.

[61] A. Yadav, A. Kumar, P.K. Singh, K. Sharma, *Integrated Ferroelectrics* **2018**, *186(1)*, 106, https://doi.org/10.1080/10584587.2017.1370331.

[62] Y. Su, H. Wei, R. Gao, Z. Yang, J. Zhang, Z. Zhong, Y. Zhang, *Carbon* **2012**, *50*, 2804, https://doi.org/10.1016/j.carbon.2012.02.045.

[63] G. Yildiz, M. Bolton-Warberg, F. Awaja, *Acta Biomaterialia* **2021**, *131*, 62, https://doi.org/10.1016/j.actbio.2021.06.047.

[64] Z. Shi, X.F. Li, H. Bai, W.W. Xu, S.Y. Yang, Y. Lu, J.J. Han, C.P. Wang, X.J. Liu, W.B. Li, *Heliyon* **2016**, *2*, e00094, https://doi.org/10.1016/j.heliyon.2016.e00094.

[65] A.K. Pathak, S.R. Dhakate, *Journal of Polymer Science* **2021**, *59*, 84, https://doi.org/10.1002/pol.20200442.

[66] A.M. Díez-Pascual, M.A. Gómez-Fatou, F. Ania, A. Flores, *Prog. Mater. Sci* **2015**, *67*, 1, https://doi.org/10.1016/j.pmatsci.2014.06.002.

[67] R.F. Gibson, *Compos. Sci. Technol* **2014**, *105*, 51, https://doi.org/10.1016/j.compscitech.2014.09.016.

[68] M.L.B. Palacio, B. Bhushan, *Materials Characterization* **2013**, *78*, 1, https://doi.org/10.1016/j.matchar.2013.01.009.

[69] M. Nowak, M. Maj, *Arch. Civ. Mech. Eng.* **2018**, *18(2)*, 630, https://doi.org/10.1016/j.acme.2017.10.005.

[70] W. Kunath, F. Zemlin and K. Weiss K., *Optik* **1987**, 76, 122.

[71] P. Trucano, R. Chen, *Nature* **1975**, *258*, 136, https://doi.org/10.1038/258136a0.

10.1002/cnma.202400488

WILEY VCH

RESEARCH ARTICLE

Entry for the Table of Contents